Constrained Invasion Percolation Model: Growth via Leath Bursts and the Origin of Seismic b-Value

John B. Rundle,[1,2,3,*] Ronaldo Ortez,[1,†] Joachim Kønigslieb,[1,‡] and Donald L. Turcotte[2,§]
[1]*Department of Physics, One Shields Avenue, University of California, Davis, California 95616, USA*
[2]*Department of Geology, One Shields Avenue, University of California, Davis, California 95616, USA*
[3]*Santa Fe Institute, Santa Fe, New Mexico 87501, USA*

(Received 17 July 2019; accepted 27 November 2019; published 13 February 2020)

We analyze a new model for growing networks, the constrained Leath invasion percolation model. Cluster dynamics are characterized by bursts in space and time. The model quantitatively reproduces the observed frequency-magnitude scaling of earthquakes in the limit that the occupation probability approaches the critical bond percolation probability in $d = 2$. The model may have application to other systems characterized by burst dynamics.

DOI: 10.1103/PhysRevLett.124.068501

Introduction.—Many driven physical processes in nature do not occur at constant rates, but rather have a burstlike character in space and time, clustering in space and time. Examples include earthquake seismicity [1], price changes price in financial markets [2], avalanche dynamics and forest fires [3], and transcriptional bursts in genomic systems [4]. In turn, many of these systems and their associated models have been mapped onto percolation models, which is a simple model for clustering [5]. An example of this type of mapping for financial markets is described in Ref. [6]. An example for earthquake systems is discussed in Ref. [7].

Here we discuss the invasion percolation model [8] that was originally developed to describe fluid injection into a porous medium, then apply it specifically to the problem of earthquake dynamics and statistics. Invasion percolation (IP) is a variation on the standard models of site and bond percolation [5], and is a type of connected graph-theoretic model wherein the nodes and edges can represent many types of quantities.

Similar to the Leath method [9] in site percolation, one starts with a central seed site and grows the cluster outward. However, in the IP model, bonds connected to existing cluster sites are opened in order of lowest probability or bond strength first, then next-lowest, and so forth. Eventually the cluster grows to "infinity" (or a predefined maximum size). One of the characteristics of the classical IP model is that there is only one timescale, the timescale on which bonds are progressively opened.

To summarize our results, we propose a new model for burstlike dynamics, the constrained Leath invasion percolation (CLIP) model. We show that this model is loopless similar to the model in Ref. [10]. Interpreting the percolation sites as units of energy release, we show that the model reproduces the observed natural scaling of earthquakes with the correct scaling exponent in the limit that the occupation probability equals the critical bond percolation probability in $d = 2$, $p_{\rm occ} = 0.5$. Comparing these results to observed scaling of earthquakes in several geological regimes, we find good quantitative agreement.

Bursts.—One of the characteristics of the IP model is the existence of bursts. Once a strong bond is opened, fluid may enter a region where weaker bonds may exist [3,11,12]. Burst sites are defined relative to an (arbitrarily) defined burst threshold strength, usually taken to be very near the critical bond probability value $p_{\rm bc}$. A burst is defined to include all bonds that are opened sequentially, where the bond strength is less than an arbitrarily defined burst threshold strength. As a practical example, Ref. [13] associated invasion percolation bursts with resistance jumps observed in laboratory studies of mercury injection into a porous medium.

A burst begins when an opened bond strength is smaller than the arbitrarily defined threshold and ends when an opened bond strength is greater than the threshold. Because the bursts are defined in this way, the particular dynamics used to grow the cluster will determine whether the individual bursts are spatially connected as well as temporally sequential. In other words, a sequence of opened bonds may not imply that a burst is a spatially connected object.

There is no concept of time independent from the sequence of opened bonds in the classical IP model. However, with respect to earthquakes in nature, there are multiple timescales. Bursts of activity may occur episodically in time, separated by a period of repose as the system "recharges" for the next seismicity burst [1]. For a more general model, we now modify the classical IP model to allow for bursts that are both spatially and temporally localized, and in which time increments have a meaning independent of the temporal development of the bursts. Or stated in an alternate way, in our modification of the model, we allow for multiple timescales.

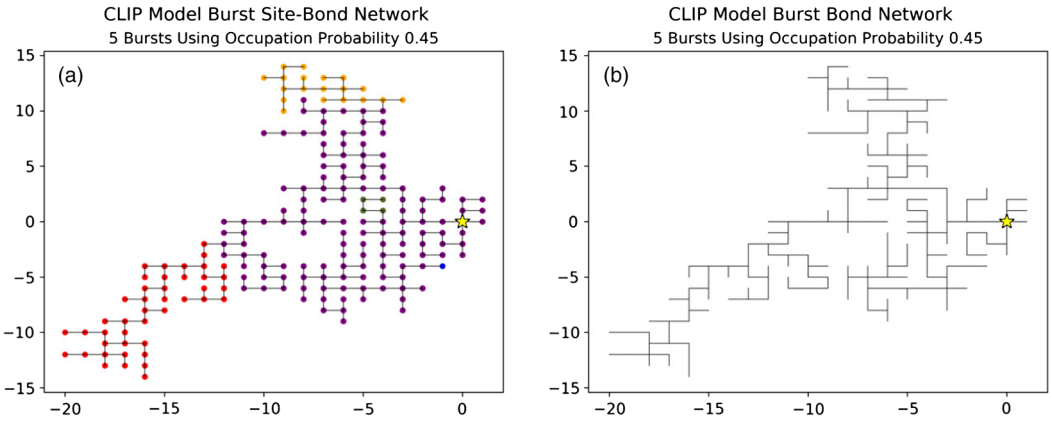

FIG. 1. Example of 5 bursts with associated open bonds. Bursts are shown as separate colors. Yellow star denotes the initial seed. (a) Bursts sites are color coded, connecting bonds are shown as dark lines. (b) Open bonds only shown as lines.

Constrained Leath invasion percolation.—In the CLIP model, we combine the idea of growing clusters via the Leath algorithm, with the constraint that each site can only be connected to the origin by means of a single pathway of bonds. We start with the "injection site" as the origin, although models with multiple injection sites could be constructed. In this model, we occupy sites in the growing cluster via Leath events or bursts. We also apply the constraint that a site can only be connected by a single path of bonds to the origin, so that multiple connection paths are not allowed, similar to constraints imposed by the method in Ref. [14]

Here we consider two timescales, an "injection scale" or long timescale on which the injections occur, and a "burst scale" or short ("instantaneous") timescale on which the bond-opening events occur. The cluster begins with growth from the origin on the first long time step.

On a square lattice in $d = 2$, the four nearest neighbor sites to the origin are first identified. As in the Leath algorithm [9], each of these four sites are tested by generating a uniformly distributed random number on (0, 1). If the random number is less than an occupation probability p_{occ}, the site is occupied and the bond between the origin and that site is opened. Testing and opening of the bonds is assumed to occur on the short timescale. This step is regarded as the first burst.

Once the testing is completed on the four nearest neighbors to the origin on the first long time step, the model proceeds to the second long time step, during which the second burst occurs. Two tests are carried out. The first test demands that the random number be less than p_{occ}, and the second test demands that an occupied site can only be connected to the origin by a single path of bonds.

The process is repeated for all later generations of bursts. The cluster grows by a series of Leath bursts, constrained by the requirement that a site is only connected to the origin once. Because the model is fundamentally constrained by bond pathways, we expect that the critical value of occupation probability should be 0.5, the value for bond percolation in $d = 2$. This expectation is borne out by simulations. Once the a burst is completed, one of the sites in the cluster is then chosen at random as the next growth site and its neighbors are identified and tested by comparing random numbers to p_{occ} and the process repeats.

An example of such a cluster composed of 5 bursts is shown in Fig. 1(a) for the value $p_{\mathrm{occ}} = 0.45$. In Fig. 1(b) it can be seen that there are no open regions in the cluster network that are totally surrounded by opened bonds and thus isolated. In the conceptual physical model, all preexisting fluid therefore has the possibility of "draining" out of the medium as bonds are opened. It can be seen that the bursts, which occur sequentially over the long timescale characteristic of fluid injection at the origin, are spatially connected. Each burst is assumed to develop over the short burst timescale.

In Fig. 2 we show the number-size non-normalized probability density functions $f(S)$ for bursts in models with two different values of occupation probability, $p_{\mathrm{occ}} = 0.45$ (a) and $p_{\mathrm{occ}} = 0.497$ (b). Figures 2(a) and 2(b) are plotted on log-log axes, so that scaling, or power law functions will appear as a straight line. Here number is the number of bursts and burst size S is the number of occupied sites in the burst. Note that this plot bins the data prior to fitting the scaling line, but the data are computed to machine precision. Quoted errors in data fits, which are calculated by least squares here and in Fig. 3, arise from the fit shown.

Both Figs. 2(a) and 2(b) are statistics for calculations with 300 000 bursts. Figure 2(a) has a shorter scaling region, whose best fit scaling line between $2.0 \geq \log_{10}(S) \geq 0.25$ has a slope of -0.806 ± 0.053. Figure 2(b), nearer to the critical occupation probability of $p_{\mathrm{bc}} = 0.5$, has a longer scaling region. The best fitting scaling line between $3.816 \geq \log_{10}(S) \geq 0.25$ is $-.667 \pm 0.013 \approx -2/3$. This latter slope in Fig. 2(b) has a significance that will become apparent shortly. We note that problems in fitting earthquake data have been discussed extensively in Refs. [15,16].

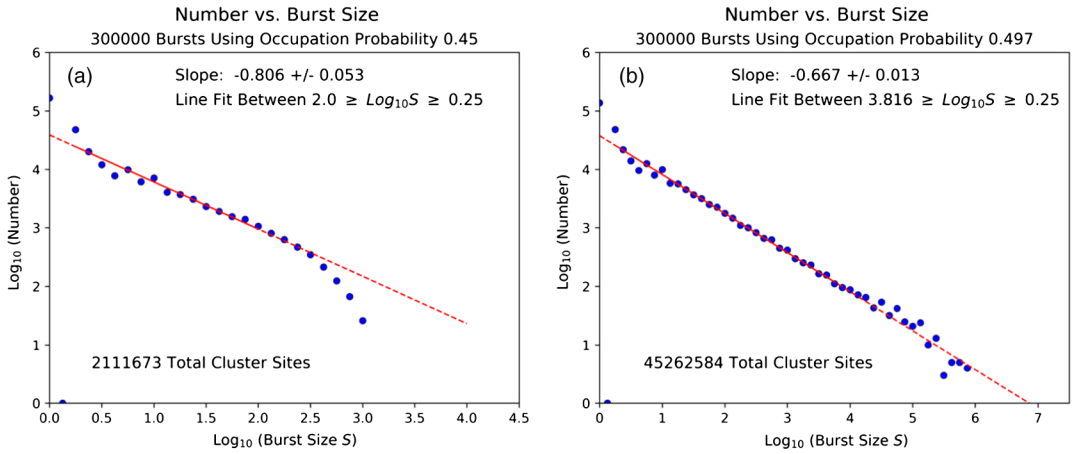

FIG. 2. Non-normalized probability density functions for number of bursts vs burst magnitude size (number of sites in a burst) on log-log axes for two values of occupation probability. Line slopes as shown. (a) Left, $p_{\mathrm{occ}} = 0.45$. (b) Right, $p_{\mathrm{occ}} = 0.497$.

The fact that the slope of the scaling line should be more negative in Fig. 2(a) than Fig. 2(b) is clear. Both plots have 300 000 bursts, and as a $p_{\mathrm{occ}} \to p_{\mathrm{bc}} = 0.5$, bursts will tend to grow larger once they are initiated. This fact is borne out by the data in Fig. 2, as (a) has 2.11×10^6 sites in the growing cluster, whereas (b) has 45.26×10^6 sites in the growing cluster. In Fig. 2(b), there are proportionally many more large clusters relative to the number of small clusters than in Fig. 2(a). As a result, the magnitude of the scaling line slope in Fig. 2(a) should be larger than the magnitude of the scaling line slope in Fig. 2(b).

For naturally occurring earthquakes, the standard in the literature is to plot the Gutenberg-Richter frequency-magnitude (or number-magnitude) relation as a non-normalized survivor distribution or exceedance distribution for earthquakes greater than a magnitude M as in Figs. 3(a) and 3(b). Earthquake magnitude is typically defined based on the energy release in earthquakes, a quantity that is characterized by the seismic moment W [17]. More specifically, the standard definition of moment magnitude M_w in SI units is

$$1.5M_w = \log_{10}(W) - 9.0, \tag{1}$$

where

$$W = \mu UA. \tag{2}$$

Here μ is the elastic shear stiffness, U is the displacement on the earthquake fault, and A is the slipped area on the fault.

We now convert the simulation data shown as the non-normalized probability density functions in Figs. 2(a) and 2(b) to non-normalized survivor (exceedance) distributions as shown in Figs. 3(a) and 3(b). Here there is no need to bin the data. In addition, rather than assuming that each site in a burst represents an element of burst area, let us assign each site to represent an element of seismic moment, consistent with the idea of CLIP as a general graph-theoretical model.

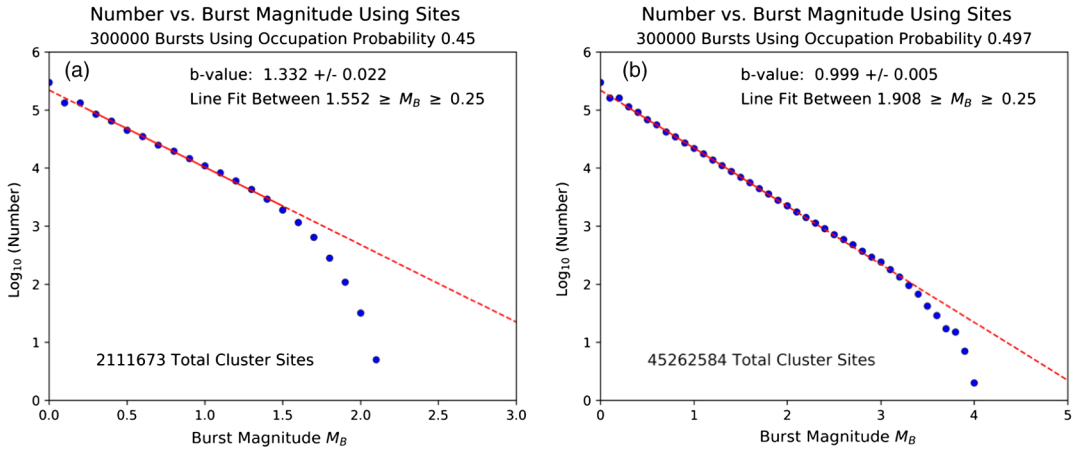

FIG. 3. Non-normalized survivor (exceedance) distributions for number of bursts vs burst magnitude (defined in the text) on log-log axes for two values of occupation probability. b-values as shown. (a) Left, $p_{\mathrm{occ}} = 0.45$. (b) Right, $p_{\mathrm{occ}} = 0.497$.

Analogous to Eq. (1), we define the burst magnitude M_B by the relation

$$1.5M_B = \log_{10}(S), \tag{3}$$

where again S is the burst size, or number of occupied sites in the burst. The results are shown in Figs. 3(a) and 3(b). Here, the slope of the scaling line on the survivor distribution plot is typically called the Gutenberg-Richter [1] b-value. Earthquake number-magnitude scaling relations are empirically found to be approximately described by the equation

$$\log_{10}(N) = a - bM_W, \tag{4}$$

where a and b are constants. Examples are shown below.

Similar to the results of Fig. 2, it can seen that the b-value of 1.332 ± 0.022 in Fig. 3(a) is larger than the b-value of 0.999 ± 0.005 in Fig. 3(b). Again, this is because the number of overall sites in the cluster is larger for larger p_{occ} having the same number of bursts. In Fig. 3(b), which was a model for which $p_{\mathrm{occ}} = 0.497$ (near $p_{\mathrm{bc}} = 0.5$), the b-value is very close to $b = 1.0$. The data in Fig. 3 were fit between $1.552 \geq M_B \geq 0.25$ for Fig. 3(a), and between $1.908 \geq M_B \geq 0.25$ for Fig. 3(b). We note that to verify the b-values, we also computed them by the maximum likelihood method and found very similar results [18–20]

More generally, for a sequence of values of p_{occ}, we find the results shown in Fig. 4. Error bars for the b-values are shown as well (68% confidence). The short dashed extension to the red line represents the extrapolation of the data to the critical value of probability $p_{\mathrm{bc}} = 0.5$. It is found that the extrapolated b-value is $b \to 1.002 \pm 0.006$ as $p_{\mathrm{occ}} \to p_{\mathrm{bc}} = 0.5$. As we discuss below, this b-value is characteristic of values seen in observed earthquake seismicity.

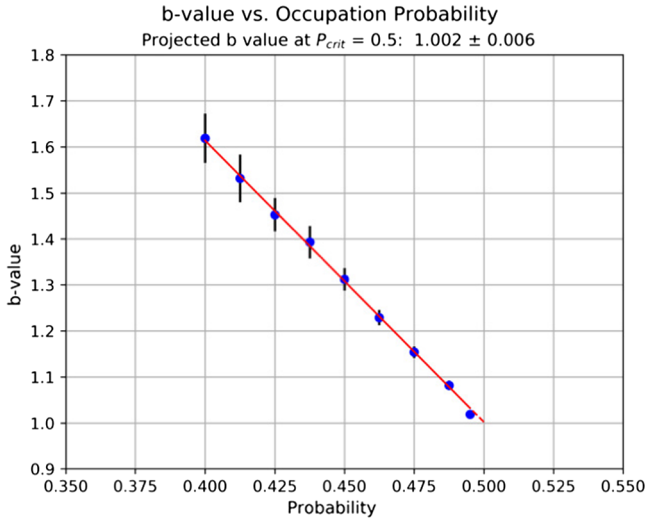

FIG. 4. b-value vs occupation probability p_{occ} for CLIP bursts. Data were fit for the range of values $0.45 \leq p_{\mathrm{occ}} \leq 0.497$. Extrapolation to the critical value $p_{\mathrm{occ}} = p_{\mathrm{bc}} = 0.5$ indicates that the b-value at criticality for the number-magnitude relation is expected to be $b = 1.002 \pm 0.006$.

To show why the limiting value of b in Fig. 4 approaches $b = 1$, we write the exceedance distribution $N(>M_B)$ for M_B in terms of the probability density function $f_B(M_B)$ as

$$N(>M_B) = \int_{M_B}^{\infty} f_B(M'_B) dM'_B. \tag{5}$$

As discussed previously, we see from Fig. 2(b) that as $p_{\mathrm{occ}} \to p_{\mathrm{bc}} = 0.5$, the probability density function $f(S)$ asymptotically approaches a power law:

$$f(S) \to cS^{-x} \quad \text{as } p_{\mathrm{occ}} \to p_{\mathrm{bc}} = 0.5, \tag{6}$$

where c is a constant and $x \to 2/3$.

Combining Eqs. (3) and (6), we find the probability density function $f_B(M_B)$ is

$$f_B(M_B) = f([S(M_B)] = c[(10^{1.5M_B})]^{-x} \to c10^{-M_B} \quad \text{as } p_{\mathrm{occ}} \to p_{\mathrm{bc}} = 0.5. \tag{7}$$

Substituting Eq. (7) into Eq. (5) we finally find that

$$N(>M_B) = \int_{M_B}^{\infty} f_B(M'_B) dM'_B = c\log_{10}10^{-M_B}. \tag{8}$$

From definition (4) and Eq. (8), we therefore see that b and $a \to \log_{10}(c \log 10)$ as the occupation probability $p_{\mathrm{occ}} \to p_{\mathrm{bc}} = 0.5$.

Earthquake data.—To compare with observed earthquake data, we show the b-value data for multiple sites and geologic regimes in Table I, for the seismicity data in circular regions. Data are from the U.S. Geological Survey. Tectonic regimes (T) are generally characterized by b-values close to $b \sim 1$, consistent with nearly critical behavior $p_{\mathrm{occ}} \sim 0.5$. In these locations, very large earthquakes (large bursts) are possible and often observed. In nature, values $b < 1$ are unusual, and are often found to be due to observational problems of detecting small earthquakes [1]. Another factor may be uneven coverage of seismometers, such as in areas that combine land, where the coverage is usually good, and oceanic areas, where the coverage is often less reliable.

Volcanic regimes (V) are generally characterized by somewhat higher noncritical probabilities and b-values near $b \sim 1.1$, since larger earthquakes are not often observed on the smaller fault systems present in volcanic edifices. Injection and fracking locations (I/F) have yet smaller fault systems, and consequently smaller earthquakes, with higher b-values near $b \sim 1.2$–1.5. But see also Refs. [21,22] for a discussion.

Discussion.—The CLIP model extends the original IP model. In earthquakes, activity is often observed to begin in a location after a period of quiescence, then progresses

TABLE I. Data for b-values in various locations and regimes (T=Tectonic; I/F=Injection/Fracking; V=Volcanic).

Location (Circle radius)	Regime	Time interval	Line fit range	b-value
Global	T	1950–2019	$6.0 \leq M_w \leq 8.0$	1.06 ± 0.02
Tokyo, Japan (1000 km)	T	1950–2019	$6.0 \leq M_w \leq 7.75$	0.99 ± 0.01
Port Mores by, Papua New Guinea (1000 km)	T	1950–2019	$6.0 \leq M_w \leq 7.5$	1.06 ± 0.02
Manila, Philippines (1000 km)	T	1950–2019	$6.0 \leq M_w \leq 7.5$	0.92 ± 0.02
Taipei, Taiwan (1000 km)	T	1950–2019	$6.0 \leq M_w \leq 7.0$	1.08 ± 0.02
Santiago, Chile (1000 km)	T	1950–2019	$6.0 \leq M_w \leq 7.5$	0.95 ± 0.02
Los Angeles, CA USA (300 km)	T	1990–2019	$1.5 \leq M_w \leq 5.0$	0.98 ± 0.01
Prague, OK, USA (200 km)	I/F	1990–2019	$3.0 \leq M_w \leq 5.0$	1.53 ± 0.02
The Geysers, CA, USA (100 km)	I/F	1990–2019	$1.25 \leq M_w \leq 5.0$	1.14 ± 0.01
Groningen, Netherlands (200 km)	I/F	1990–2019	$2.75 \leq M_w \leq 5.0$	1.26 ± 0.02
Kilauea Summit, HI, USA (200 km)	V	1990–2019	$2.75 \leq M_w \leq 5.0$	1.1 ± 0.02
Mt. Pinatubo, Philippines (200 km)	V	1990–2019	$4.75 \leq M_w \leq 6.0$	1.09 ± 0.03
Mt.Etna, Sicily (200 km)	V	1990–2019	$4.75 \leq M_w \leq 6.0$	1.09 ± 0.08

in a series of burstlike events to cluster in space and time [23–31]. These bursts include foreshock-mainshock-aftershock sequences, as well as swarms [32].

Previous papers have developed simple models for earthquakes based on percolation [5] and slider blocks [33,34]. In the mean field versions of these models, the frequency-size exponent $\tau - 1$ is generally found to have the value $\tau - 1 = 1.5$ [34], to be compared to Fig. 2. Interpreting a connected site as an element of moment release as we have assumed in this paper, one would find $b = 1.5$, compared to the observed value near $b \sim 1$.

On the other hand, using a slider block model with damage, Ref. [7] found that models could be developed in which $b \sim 1.0$. In both of these other models, τ is a constant irrespective of model parameters. As another example, the SOC model of Ref. [35] is characterized by an area-scaling exponent of $\tau - 1 \sim -1$, so it too would have $b \sim 1$. However, for all these models, the area-scaling exponents are constant, and therefore the b-value is constant.

The CLIP model, on the other hand, has a variable b-value. As the CLIP occupation probability approaches the critical value $p_{\mathrm{occ}} \to p_{\mathrm{bc}} = 0.5$, larger bursts become progressively easier to generate, leading to a lower b-value that approaches the observed value in the limit.

We note that other scaling laws characteristic of earthquakes can be obtained from the CLIP model. For example, we find that the fractal dimension of the clusters $D_f = 1.89 \pm 0.021$, in good agreement with the observationally measured value of $D_f = 1.9$ [36].

As described in many previous publications of long standing, the mobilization of pore fluids is thought to be intimately connected to the physics of earthquakes [37–45], providing possible justification for the CLIP model. The model will also allow earthquake seismicity data to be interpreted in terms of current values of burst probabilities p_{occ} [46,47].

The research conducted by J. B. R. and R. O. has been supported in part by a grant from the U.S. Department of Energy to the University of California, Davis, DOE Grant No. DE-SC0017324. We are also grateful for thoughtful reviews by Professor I. Main and an anonymous reviewer. Data for the analysis were obtained from the USGS global earthquake catalog, available in Ref. [48].

*rundle@ucdavis.edu
†raortez@ucdavis.edu
‡joachim.koenigslieb@gmail.com
§dlturcotte@ucdavis.edu

[1] C. H. Scholz, *The Mechanics of Earthquakes and Faulting* (Cambridge University Press, Cambridge, 2018).
[2] R. N. Mantegna and H. E. Stanley, *An Introduction to Econophysics, Correlations and Complexity in Finance* (Cambridge University Press, Cambridge, 2004).
[3] M. Paczuski, S. Maslov, and P. Bak, Phys. Rev. E **53**, 414 (1996).
[4] K. B. Halpern, S. Tanami, S. Landen, M. Chapal, L. Szlak, A. Hutzler, A. Nizhberg, and S. Itzkovitz, Mol. Cell **58**, 147 (2015).
[5] D. Stauffer and A. Aharony, *Introduction to Percolation Theory* (Taylor & Francis, London, 2018).
[6] D. Stauffer and D. Sornette, Physica A (Amsterdam) **271**, 496 (1999).
[7] C. A. Serino, K. F. Tiampo, and W. Klein, Phys. Rev. Lett. **106**, 108501 (2011).
[8] D. Wilkinson and J. F. Willemsen, J. Phys. A **16**, 3365 (1983).
[9] P. Leath, Phys. Rev. B **14**, 5046 (1976).
[10] J. Q. Norris, D. L. Turcotte, and J. B. Rundle, Phys. Rev. E **89**, 022119 (2014).
[11] S. Roux and E. Guyon, J. Phys. A **22**, 3693 (1989).
[12] S. Maslov, Phys. Rev. Lett. **74**, 562 (1995).
[13] J.-N. Roux and D. Wilkinson, Phys. Rev. A **37**, 3921 (1988).
[14] C. P. Stark, Nature (London) **352**, 423 (1991).
[15] J. Greenhough and I. Main, Geophys. Res. Lett. **35** (2008).
[16] A. F. Bell, M. Naylor, and I. G. Main, Geophys. Res. Lett. **40**, 2585 (2013).
[17] T. C. Hanks and H. Kanamori, J. Geophys. Res.: Solid Earth **84**, 2348 (1979).

[18] K. Aki, Bull. Earthq. Res. Inst., Tokyo Univ. **43**, 237 (1965).
[19] T. Utsu, Geophys. Bull. Hokkaido Univ. **13**, 99 (1965).
[20] Y. Shi and B. A. Bolt, Bull. Seismol. Soc. Am. **72**, 1677 (1982).
[21] N. S. Roberts, A. F. Bell, and I. G. Main, J. Volcanol. Geotherm. Res. **308**, 127 (2015).
[22] N. S. Roberts, A. F. Bell, and I. G. Main, Geophys. Res. Lett. **43**, 4288 (2016).
[23] J. Gardner and L. Knopoff, Bull. Seismol. Soc. Am. **64**, 1363 (1974).
[24] P. Reasenberg, J. Geophys. Res.: Solid Earth **90**, 5479 (1985).
[25] D. Marsan and O. Lengline, Science **319**, 1076 (2008).
[26] I. Zaliapin and Y. Ben-Zion, J. Geophys. Res.: Solid Earth **118**, 2865 (2013).
[27] I. Zaliapin and Y. Ben-Zion, Bull. Seismol. Soc. Am. **106**, 846 (2016).
[28] I. Zaliapin and Y. Ben-Zion, Geophys. J. Int. **207**, 608 (2016).
[29] I. Zaliapin, A. Gabrielov, V. Keilis-Borok, and H. Wong, Phys. Rev. Lett. **101**, 018501 (2008).
[30] A. Peresan and S. Gentili, Phys. Earth Planet. Inter. **274**, 87 (2018).
[31] B. Luen and P. B. Stark, Geophys. J. Int. **189**, 691 (2012).
[32] C. S. Weaver and D. P. Hill, Pure Appl. Geophys. **117**, 51 (1978).
[33] J. B. Rundle and W. Klein, J. Stat. Phys. **72**, 405 (1993).
[34] W. Klein, M. Anghel, C. Ferguson, J. Rundle, and J. S. Martins, Geophys. Monogr. Am. Geophys. Union **120**, 43 (2000).
[35] P. Bak, C. Tang, and K. Wisenfeld, Phys. Rev. A **38**, 364 (1988).
[36] M. Sahimi, M. C. Robertson, and C. G. Sammis, Phys. Rev. Lett. **70**, 2186 (1993).
[37] A. Nur and J. R. Booker, Science **175**, 885 (1972).
[38] R. Sibson, Nat. Phys. Sci. **243**, 66 (1973).
[39] R. H. Sibson, Earthquake Predict. Int. Rev. **4**, 593 (1981).
[40] R. Sibson, Tectonophysics **211**, 283 (1992).
[41] R. Sibson, J. M. M. Moore, and A. Rankin, J. Geol. Soc. **131**, 653 (1975).
[42] R. M. Wood, Geol. Soc., London, Spec. Publ. **78**, 85 (1994).
[43] G. Peltzer, P. Rosen, F. Rogez, and K. Hudnut, Science **273**, 1202 (1996).
[44] M. M. Scuderi and C. Collettini, Sci. Rep. **6**, 24852 (2016).
[45] M. Scuderi, C. Collettini, and C. Marone, Earth Planet. Sci. Lett. **477**, 84 (2017).
[46] R. Ortez *et al.* (to be published).
[47] J. Konig *et al.* (to be published).
[48] https://earthquake.usgs.gov/earthquakes/search/.